TRENDS IN SCIENCES 2025; 22(11): 10073
https://doi.org/10.48048/tis.2025.10073 RESEARCH ARTICLE

Microstructure and Dispersion Parameters of Hybrid PMMA/(TiO_2-ZrC) Electrospun Nanofibers for Optoelectronics and Antimicrobials Purposes

Eman J. Husien and Fouad Sh. Hashim*

Department of Physics, College of Education for Pure Science, University of Babylon, Iraq

(*Corresponding author's e-mail: pure.foaad.shakir@uobabylon.edu.iq)

Received: 2 March 2025, Revised: 18 March 2025, Accepted: 25 March 2025, Published: 1 August 2025

Abstract

The method of solution electrospinning under the main conditions of 13 kV, 0.5 mL per h flow rate, and collector rotating 250 per min was used to fabricate PMMA composite nanofibers using mixed (TiO_2-ZrC) nanomaterials (1:1 wt.%) as a filler in varying concentrations: 2, 4, and 6 % to utilize in futuristic photonics applications. FTIR results confirm strong interactions between the PMMA matrix and (TiO_2-ZrC). Morphological analysis performed through FESEM confirmed the average diameters of the nanofibers, which showcased 82.37 nm for the polymer and increased to 139.59 nm at a weight of 6 %, while their rough surfaces are transformed into smoother ones depending on the addition of nanomaterials. EDXs provide insights into the element's composition of the PMMA encapsulating by TiO_2 and ZrC. A decrease in light transmittance in the UV region gives a positive indication of the protective action in solar cells. Increasing the TiO_2-ZrC nanoparticle content by 6 wt.% gradually improved the indirect transition band gap ($E_{g\,indir}^{opt}$) for the allowed and forbidden from 3.5 and 3.2 eV for the pure polymer to 2.8 and 2.18 eV. This finding is a positive indication of its use in many optoelectronic devices. The theoretical Wemple-DiDomenico model has been implemented to evaluate the refractive index (ns), the oscillation energy (Eos), and the dispersion energy (Ed). Moreover, (TiO_2-ZrC) demonstrated upper optical activity and elevated DNA decay efficiency than PMMA, validating their higher efficiency as an optical and antimicrobial agent.

Keywords: PMMA, TiO_2, ZrC, Nanofiber, Electrospinning, Optical properties

Introduction

Nanomaterials exhibit unique properties due to their small size and large surface area, making them useful in various fields [1]. Due to academic and industrial interests, their presence with inorganic polymeric materials has been important during the last 2 decades. Due to the significant improvements, it adds to the properties, such as mechanical, thermal, optical, and electrical properties of different composite membranes and recent developments in electrospinning technology, different types of polymers/inorganics and their nanocomposites have been produced [2,3].

Poly methyl methacrylate (PMMA), a synthetic resin derived from the polymerization of methyl methacrylate with the empirical formula ($C_5H_8O_2$), exhibits a glass transition temperature of 105 °C and demonstrates inadequate mechanical properties, including low impact resistance and susceptibility to fatigue failure. However, their optical properties, including clarity, index of refractive, haze, and light transmission, are critical features that make them uniquely advantageous for several design and engineering applications, including optics, lighting, and displays [4].

Titanium dioxide (TiO_2) is a semiconducting transition material. It shows unique characteristics, such as easy control, low cost, nontoxicity, wide energy gap (3.0 to 3.2 eV), and great resistance, which can absorb ultraviolet rays and become irritated. The unique physiochemical features of metal oxide NPs, such as (TiO_2), have made them widely used in biological

applications in recent decades [5]. According to several publications, TiO_2 NPs have been among the most investigated TiO_2 NPs due to their photocatalytic and antibacterial activity, which exerts good bio-related action against bacterial contamination [6]. Zirconium carbide (ZrC) is an attractive material for optical applications due to its excellent optical performance in the infrared range and high stability even at elevated temperatures. Doping ZrC nanoparticles with different elements has emerged as an effective strategy to improve their optical performance with a wide band gap of about 2.9 eV [7]. ZrC NPs have garnered attention due to their cubical shape, strong bands, stability, and applicability in biomedicine and drug delivery. Ongoing studies focus on the impact of different media on the energy gap of ZrC NPs, as the energy gap is size and shape-dependent and influenced by the surrounding medium [8]. Studies have demonstrated significant interest in nanoparticles due to their potential for various uses, such as their antibacterial properties.

Electrospinning is an economical and accurate technique for generating polymeric fibers with diameters spanning the nano-to-micron range, yielding a substantial length-to-diameter ratio [9]. Consequently, electro-spun polymer nanofibers are appealing materials for diverse applications, including tissue engineering scaffolds, filtration media, protective garments, and antimicrobial membranes [9]. It is possible to vary the carrier concentration in the matrix material by adding many elements or oxides to develop improved composite applications [10]. By electrospinning solutions with N-N dimethyl for maimed (DMF) as the solvent, Chen *et al.* [11] were able to successfully create PMMA/silica nanocomposite fibers that had up to 20 weight percent silica. Kanth *et al.* [12] successfully fabricated porous PMMA substrates with immobilized TiO_2 NPs in fiber shapes. These substrates were then evaluated to illustrate the influence of pollutant movement and light accessibility on the total photo-catalytic performance. Sallomi *et al.* [13] succeeded in the electrospinning method to prepare PMMA/TiO_2 nanofibers. The influence of collector rotation speed on the diameters, morphology, and structural characteristics of the synthesized PMMA/TiO_2 nanofibers was examined. The primary aims of this study are to fabricate nanofibers using the electrospinning technique with PMMA and a mixture of TiO_2 and ZrC, and to analyze their morphological, optical, and dispersion characteristics for prospective applications in various optoelectronic and antimicrobial fields.

Materials and methods

Materials

White powder of TiO_2, 99 %, < 80 nm, 79.8658 $g.mol^{-1}$, and black powder ZrC, 99 %, < 80 nm, 103.235 $g.mol^{-1}$) were bought and acquired from US Research Nanomaterial's, Inc., USA. PMMA [CH_2=C (CH3) $COOCH_3$], with a purity of minimum assay around 98 % with MW~120,000 $g.mol^{-1}$, was bought from SIGMA-ALDRICH (Germany). DMF, purity > 90 %, was selected to dissolve PMMA polymer obtained from Alpha Chemical, India.

Preparation the solution of PMMA / (TiO_2-ZrC)

The preparation of a nanocomposite (NC) solution from PMMA / (TiO_2—ZrC) was described by dissolving 1 g of PMMA in 20 mL of DMF and stirring for 1 h at 50 °C using a magnetic stirrer. The (TiO_2—ZrC) NPs were added in a 1:1 ratio at weights equal to 2, 4, and 6 % with continuous mixing and using ultrasound many times (at least thrice) to achieve homogeneity. The solution now undergoes electrospinning to fabricate the nanofibers.

Preparation of PMMA/ (TiO_2- ZrC) nanofibers

The synthesis of PMMA/(TiO_2-ZrC) composite nanofibers is delineated as follows: An aluminum foil of 10×25 cm^2 was encased around the drum collector, and requisite modifications were implemented to the needle tip-to-collector distance. The solution was transferred into a 5 mL glass syringe sealed with an 18-gauge blunt cannula. The electrospinning tests were performed at a flow rate of 0.5 mL per h and 13 kV within a sealed environmental room illuminated by UV light, as depicted in **Figure 1**. A metal capillary needle was employed to transfer the prepared solution into a 5-milliliter syringe, positioned 8 cm from a metal cylinder rotating at 250 revolutions per min. The film thicknesses measured approximately 20 μm.

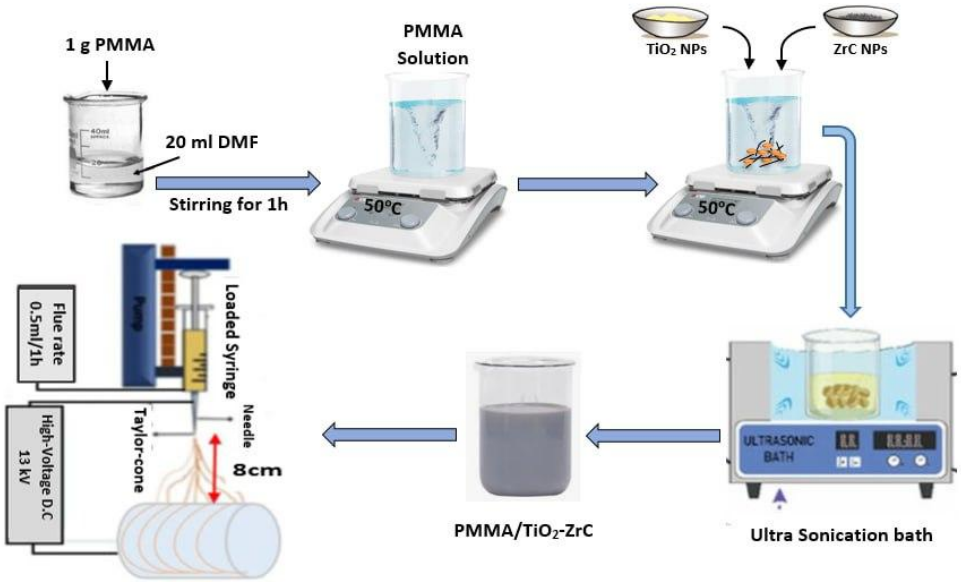

Figure 1 Diagram of the electrospinning to manufacturing nanofibers.

Characterization

The chemical composition of the PMMA/(TiO_2-ZrC) composite nanofibers was characterized using FTIR spectroscopy (Bruker company, German origin, type vertex-70) at (4000 - 400) cm^{-1}. The surface morphology was examined using FESEM (MIRA3 TESCAN). EDXs imparted insights into the chemical composition of the PMMA encapsulating TiO_2 and ZrC and utilizing image processing software to calculate the sizes of nanofibers in detail. The sorption behavior was examined by (Shimadzu UV-1800) spectrophotometer over a wavelength of (200 to 1100 nm) range.

Results and discussion

FTIR spectra

Figure 2 displays the FTIR spectroscopy of PM and its nanocomposite with different weight percentages of a mixed (TiO_2-ZrC) in the wavenumber range of (600 - 4000) cm^{-1}, recorded at room temperature. The peaks seen at 2950.28, 1721.82, 1434.91, ~1240.35, and ~1144.15 cm^{-1} are due to the asymmetric stretching of the CH_2 group Tommasini *et al.* [14], carbonyl group (C=O) Salloomi *et al.* [13], Torrisi *et al.* [15], C-H deformation Ali *et al.* [16], C-O stretching and skeletal vibrations coupled to the C-H deformations Godiya *et al.* [17], respectively. The peaks at 986.43, 838.24, and 748.25 cm^{-1} are customized to CH_2 rocking mode [15]. Also, it can be seen at around 662.26 cm^{-1} new clear bands show when the concentration of (TiO_2-ZrC) is high enough 4wt.%, which can be customized to vibration modes of Ti-O-Ti and Zr-O-Zr [18-20]. The results related to the FTIR technique indicate that the slight deviation in the peak positions towards greater or smaller wavelengths occurs as a result of compensation or the effect of solvents. This suggests physical, structural changes represented by the strong hydrogen bonding interaction between the polymer matrix and additive nanomaterials. Also, from such a figure, it is clear that increasing the weight percentage of additive NPs, the regularity of the nanofibers, and their diameters do not affect the functional groups of PMMA/ (TiO_2-ZrC) nanofibers. This may be because the change in the physical dimensions of the nanofibers does not involve chemical reactions affecting the functional groups of the PMMA/(TiO_2-ZrC) nanofibers [21].

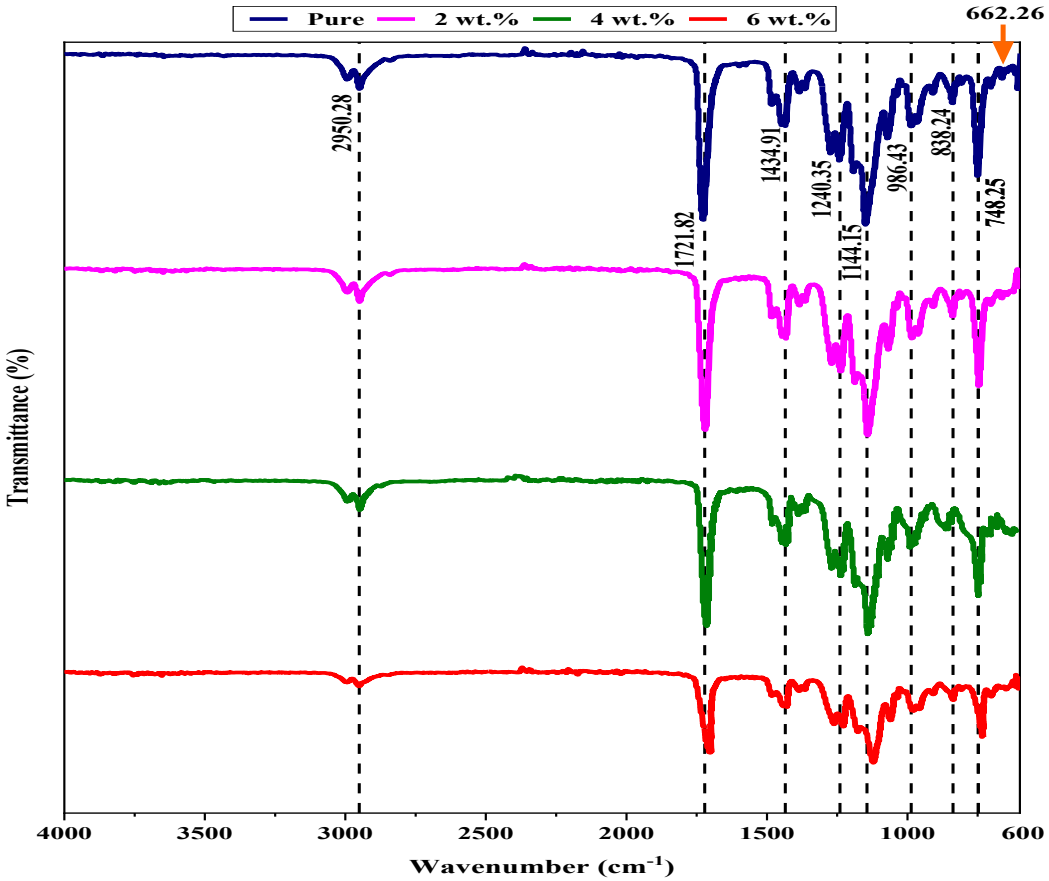

Figure 2 The FTIR spectra of the PMMA/ (TiO_2-ZrC) composite nanofibers.

Morphology of (TiO_2-ZrC) loaded PMMA composite nanofibers

Our images shown in **Figures 3 - 6** are the FESEM (taken at magnification15 kx and inset 60 kx), histograms of diameters with Gaussian distribution, and EDXs for pure solution PMMA and its nanocomposite with different weights 2, 4, and 6 % of a mixed (TiO_2-ZrC) NPs. The nanofibers from pure solution PMMA had a porous and rough surface, as mentioned in the research Kanth *et al*. [12], while their rough surfaces were transformed into smoother ones depending on the addition of nanomaterials. The average diameter of the nanofibers was approximately 82.377 nm for a pure PMMA and increased to 96.083, 100.955, and 139.589 nm for NCs with different weights 2, 4, and 6 % (TiO_2-ZrC), respectively. The consistent rotation speed of the collector correlates with the rise in fiber diameter, attributable to the additive nanoparticles that altered the charge density and viscosity of the solution, hence elucidating the variation in fiber diameter [21].

Through the typical analysis of EDXs (dominant peak represented by aluminum foil on which the film is deposited) performed on the PMMA and its composite nanofibers, shown in part c of **Figure 3**, it was found that the typical peaks are associated with carbon (C), oxygen (O), titanium (Ti) and zirconium (Zr). This suggests the possibility of obtaining nanocomposites from PMMA/ (TiO_2-ZrC).

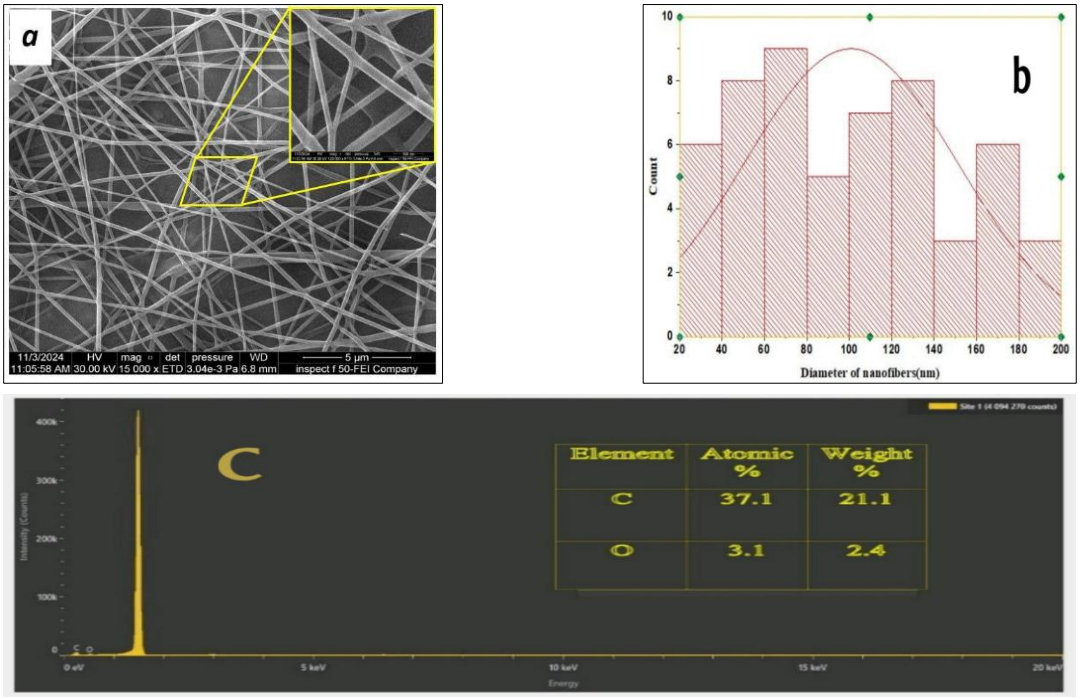

Figure 3 (a) FESEM images, (b) Gaussian distribution, and (c) EDXs of the pure PMMA.

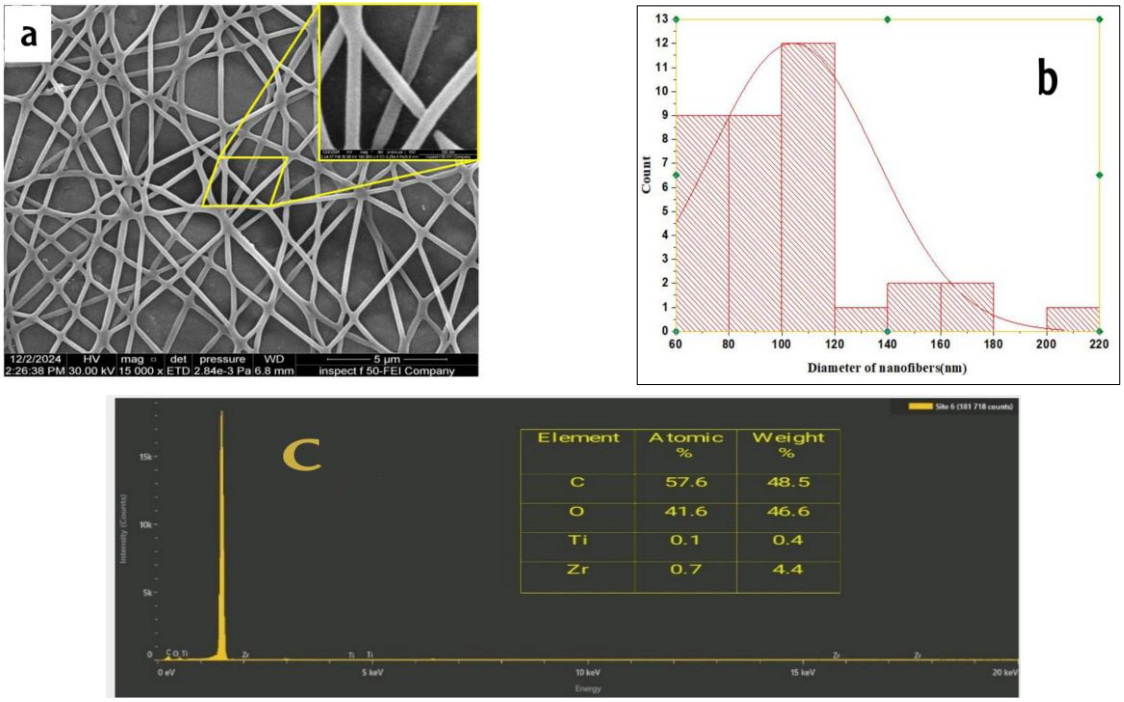

Figure 4 (a) FESEM images (b) Gaussian distribution, and (c) EDXs of PMMA/2wt.% (TiO_2-ZrC).

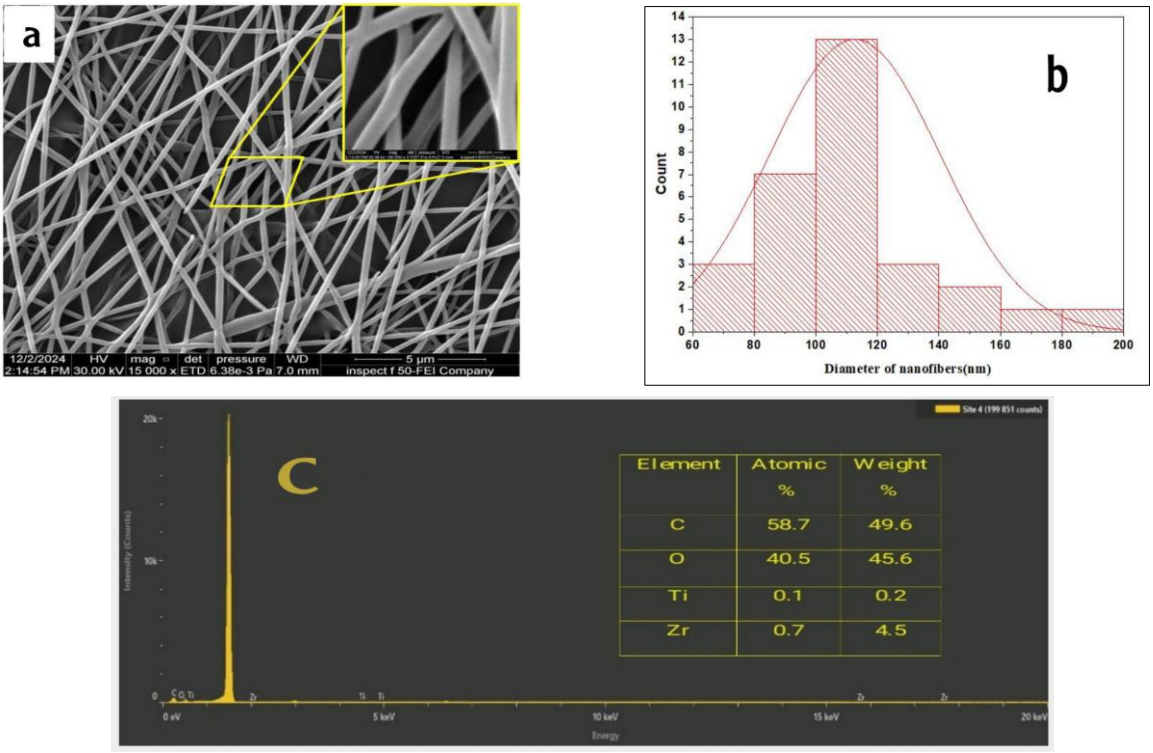

Figure 5 (a) FESEM images, (b) Gaussian distribution, and (c) EDXs of PMMA/4wt.% (TiO_2-ZrC).

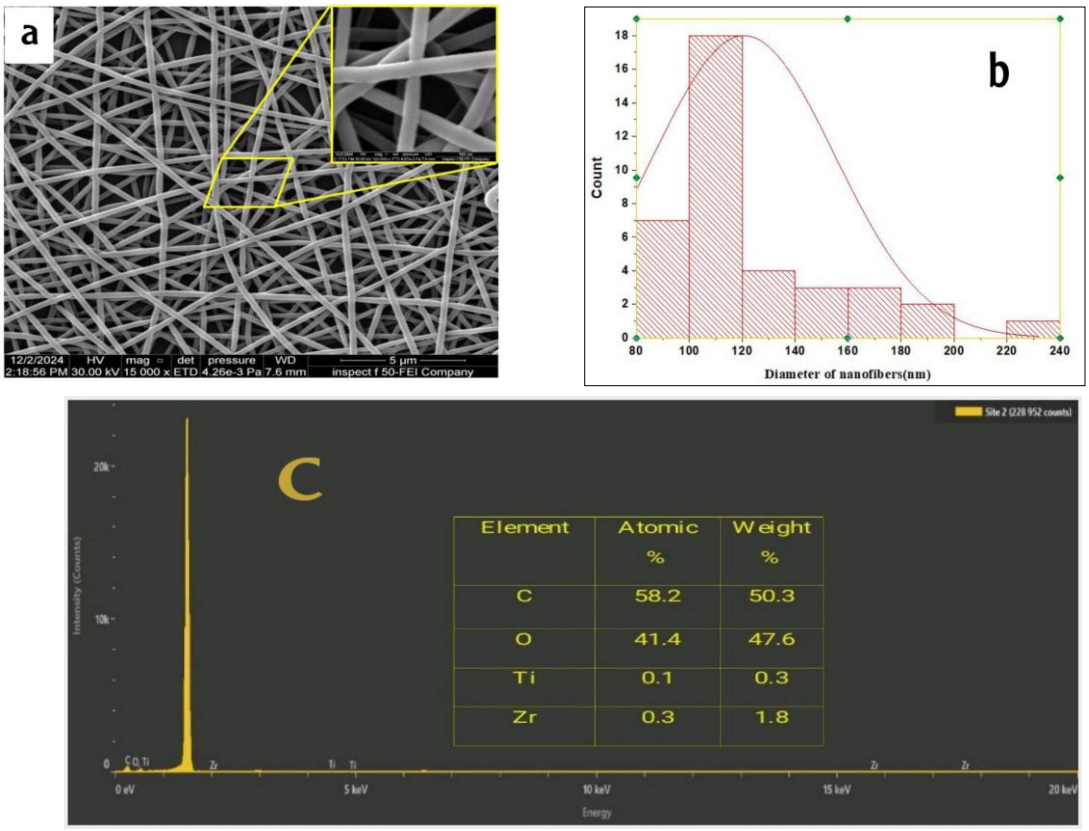

Figure 6 (a) FESEM images, (b) Gaussian distribution, and (c) EDXs of PMMA/6wt% (TiO_2-ZrC).

UV-visible spectrophotometer

Figure 7 depicts the transmittance spectra of pure PMMA and 3 different weight 2, 4, and 6 % (TiO_2 - ZrC) nanocomposites introducing into polymer matrix. The transmittance of pure PMMA film along the visible region is found to be in the range 94 - 96.5 %. At 6 wt.%

the transmittance values decrease to 87.6 % at the wavelength approaches 560 nm, since the increase of nanomaterial's could increase light absorbance and decrease transmittance [22,23]. The reduction in light transmittance in the UV spectrum suggests a favorable protective effect on solar cells.

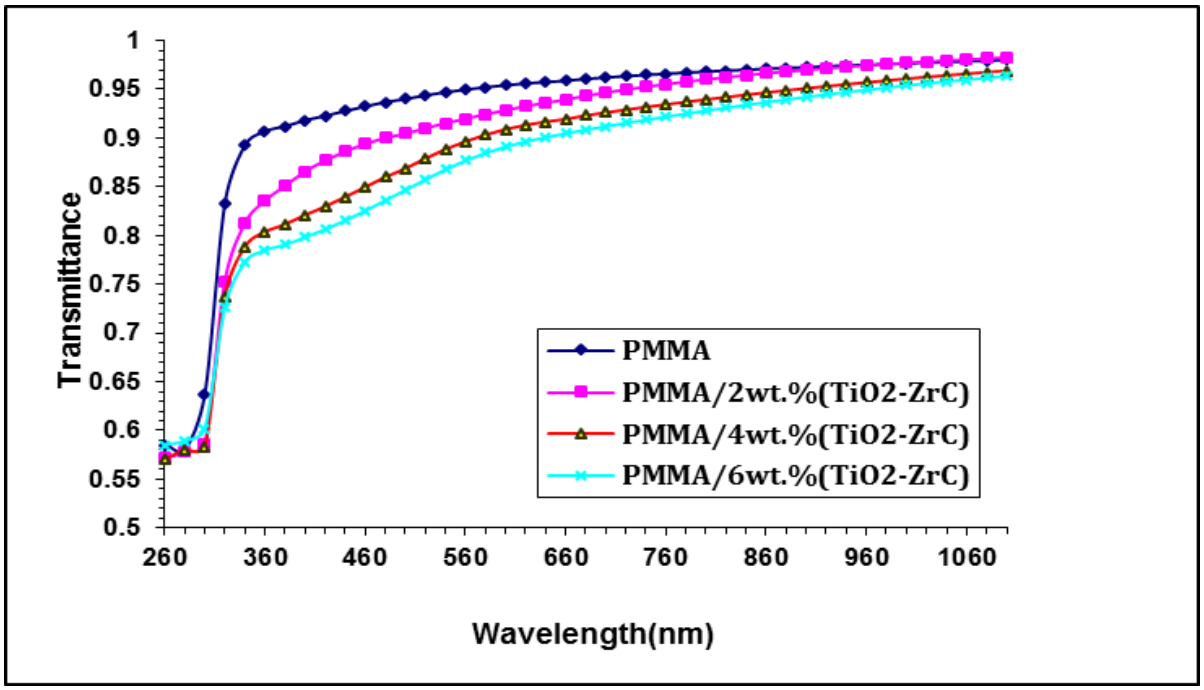

Figure 7 UV-Vis transmittance spectra of pure PMMA and 3 different (TiO_2-ZrC) nanocomposites.

The type of electronic transitions between extended bands can be identified from the absorption coefficient (α) calculation [24].

$$\alpha = 2.303\ (\frac{A}{t})\ \text{(A absorption and t thickness)} \quad (1)$$

From α calculation, Urbach tail energy (E_U) can be found from the relation, which is shows inclusions and instabilities in a polymer matrix [25,26].

$$\ln \alpha = \ln \beta o\ + \frac{h\upsilon}{Eu}\ \text{(hυ signifies the energy of the photon)} \quad (2)$$

The predestined optical band gap (E_g^{opt}) were evaluated from the following relation [27].

$$\alpha h\upsilon = B\ (h\upsilon - E_g^{opt}\ )^{\,n} \quad (3)$$

where B is defined as a constant, and the n takes a variable values of 2 and 3 for allowed and prohipted indirect transitions.

The absorption coefficient values in **Figure 6(a)** were less than $10^4\ cm^{-1}$ indicated occur indirect transfers in all prepared samples [28]. The E_U values are obtained by fitting the graph's straight section, which is the inverse of its slope, as shown in **Figure 6(b)**, respectively, 0.35, 0.51, 0.59, and 0.72 eV for pure PMMA and 3 mixed different weight 2, 4, and 6 % (TiO_2-ZrC) NCs. The allowed and forbidden transitions band gap ($E_{g\,indir}^{opt}$) decreased from 3.5 and 3.2 eV (pure polymer) to 2.8 and 2.18 eV at a weight of 6 % nano additives, as shown in **Figure 8** and tableted in **Table 1**. The chaotic structure formed by the polymer chains upon solidification and the presence of TiO_2 and ZrC nanomaterials leads to the formation of disordered atoms and structure-related defects that can lead to the emergence of local states that act as donor centers close to or at the conduction band level, causes to increase in the Urbach tail. Consequently, the optical energy gap decreases. This finding provides a positive indication for use in many optoelectronics devices, like photovoltaic cell applications.

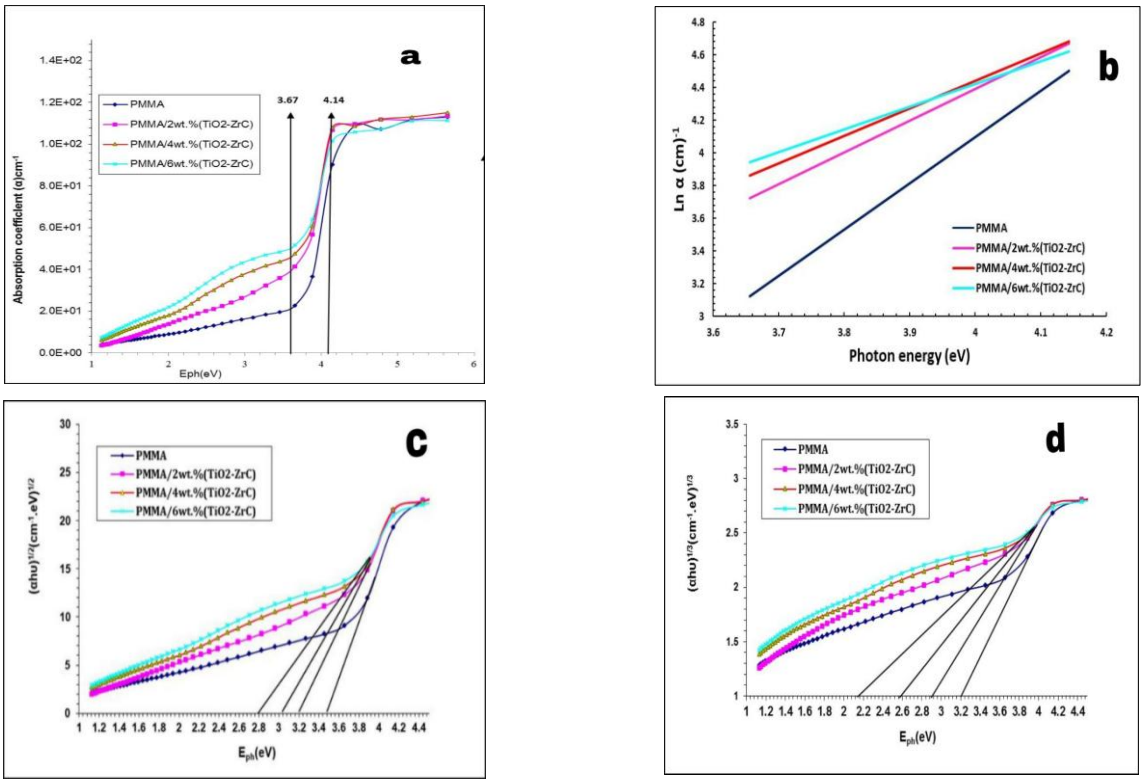

Figure 8 (a) Spectral distributions of α, (b) E_U, (c) and (d) allowed and forbidden indirect transition ($E_{g\ indir}^{opt}$) for pure PMMA and 3 different mixed (TiO_2-ZrC) NCs.

Table 1 The values of both allowed and forbidden indirect transitions and Urbach energy (E_U).

(TiO_2-ZrC) wt.%	**Allowed $E_{g\ indir}^{opt}$ (eV)**	***Forbidden* $E_{g\ indir}^{opt}$ (eV)**	**E_U (eV)**
0	3.50	3.2	0.35
2	3.20	2.95	0.51
4	3.00	2.6	0.59
6	2.80	2.18	0.72

The optical conductivity (σ_{op}) has been specified using the following relation [29].

$$\sigma_{op} = \alpha\ n\ c/4\pi \qquad (c \text{ speed of light}) \qquad (4)$$

Optical conductivity is closely linked to the optical band gap, making it an essential field of investigation.

The relationship between σ_{op} and λ for PMMA and 3 different mixed (TiO_2-ZrC) NCs is shown in **Figure 9**. σop depends on the α and can be noticing a sharp increase in the UV region. The σ_{op} was determined to transmit in the Vis and NIR ranges. The augmentation of inorganic filler quantity leads to an elevation in the density of localized states within the forbidden energy gap, hence boosting α and subsequently σ_{op} [30].

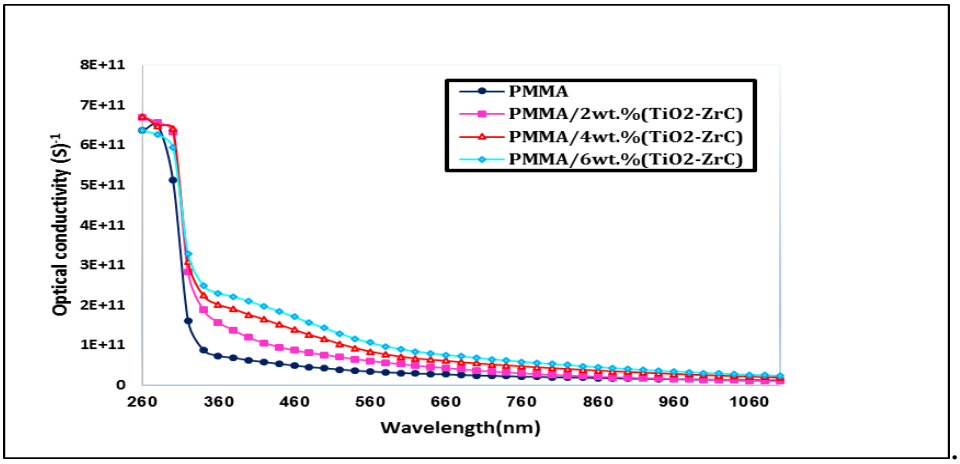

Figure 9 Optical conductivity for PMMA and 3 different mixed (TiO_2-ZrC) NCs.

Parameters of dispersion energy

The Wemple - DiDomenico model include, the energy of single oscillator (Eos), the energy of dispersion (Ed), and the photon energy (hυ) [31]. The Wemple DiDomenico model can be expressed mathematically as follows [31].

$$(n^2-1)^{-1} = \frac{E_{os}}{E_d} - \frac{1}{E_{os}\,E_d}(h\upsilon)^2 \quad (5)$$

The plotted data from $(n^2-1)^{-1}$ as a function of $(h\upsilon)^2$ for PMMA with various ratios of (TiO_2-ZrC), forms a straight line with a y-intercept equal to (E_{os} / E_d) and a slope equal to ($1/E_{os}E_d$), as in **Figure 10**. The calculated values of E_{os} and E_d displayed in **Table 2**. The energy parameter E_{os} of PMMA reduces with the addition of (TiO_2-ZrC), which corresponds to the decrease in the optical energy gap. Moreover, E_d values increase, which indicates that the inclusion of (TiO_2-ZrC) improved the optical transition intensity as a result of atomic diffusion to interstitial locations in the PMMA polymer [32].

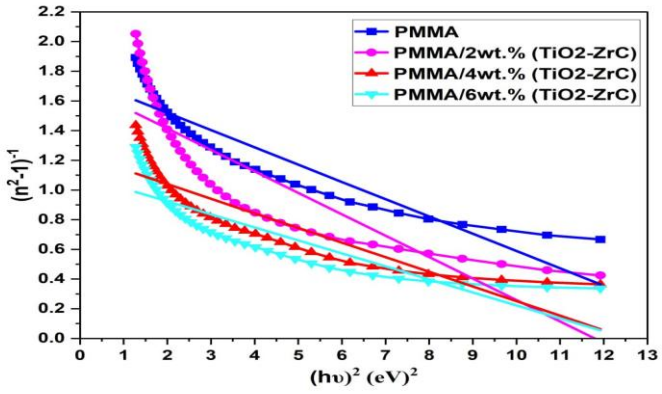

Figure 9 Plot of $(n^2-1)^{-1}$ vs $(h\upsilon)^2$ for PMMA and 3 different mixed (TiO_2-ZrC) NCs.

The values of E_{os} and E_d can be used to calculate the dielectric constant (ε_s) and the static refractive index (n_s) from the following equation [33]:

$$\varepsilon_s = n_s^2 = 1 + \frac{E_d}{E_{so}} \quad (6)$$

These values (listed in **Table 2**) increased as the content of nanoaditives in the matrix increased. Furthermore, using (E_d and E_{os}), it is possible to compute the optical moments (M_{-1} and M_{-3}) for the current nanofiber films. These moments were determined as follows equations [34].

$$E_{os}^2 = \frac{M_{-1}}{M_{-3}} \quad \text{And} \quad E_d^2 = \frac{M_{-1}^3}{M_{-3}} \tag{7}$$

$$M_{-1} = \frac{E_d}{E_{os}} \quad \text{And} \quad M_{-3} = \frac{M_{-1}}{E_{os}^2} \tag{8}$$

By rearranged these equations, one may obtain [35]:

Increasing the (TiO_2-ZrC) content resulted in a boost of the optical spectra moments, thereby strengthening the optical transitions.

Table 2 The dispersion parameters for PMMA and 3 different mixed (TiO_2-ZrC) NCs.

(TiO_2-ZrC) wt.%	**E_{OS} (eV)**	**E_d (eV)**	**n_s**	**ε_s**	**M_{-1}**	**M_{-3}**
0	3.88	2.21	1.25	1.5625	0.57	0.038
2	3.43	2.02	1.26	1.5876	0.59	0.049
4	3.54	2.86	1.34	1.7956	0.81	0.064
6	3.55	3.22	1.38	1.9044	0.91	0.072

The antibacterial activity

When a material exhibits certain optical properties upon contact with bacteria, this may indicate that certain chemical or physical processes are taking place that contribute to the material's antibacterial activity and may enhance its efficiency [36]. The PMMA and 3 different mixed (TiO_2-ZrC) NCs were assessed for antibacterial activities against 4 bacterial strains, gram-negative *Escherichia coli*, *klebsiella aurous*, *Pseudolysogeny*, and gram-positive *Staphylococcus aurous*, as manifested in **Figure 10**. These selected bacteria because they are among the most common causes of clinically acquired infections, along with, delayed healing of soft tissue burn wounds [37]. The maximum inhibitory power of the bacterial zone (22 mm) against *Staphylococcus aurous* was recorded when (TiO_2-ZrC) nanoparticles attained 6 wt.%, as illustrated in the histogram of **Figure 11**. These results can be interpreted in the case of PMMA/(TiO_2-ZrC) composite nanofibers the positively charged ion of a metallic element generated from nanoparticles cross-react with proteins at the membrane of the cell barrier, and nucleic acids (DNA), causing alterations in their structure and inhibiting microbial reproduction. Also, reactive oxygen species (ROS) are responsible for taking up nanoparticles, which causes the mechanical breakdown of the cell membrane [38,39].

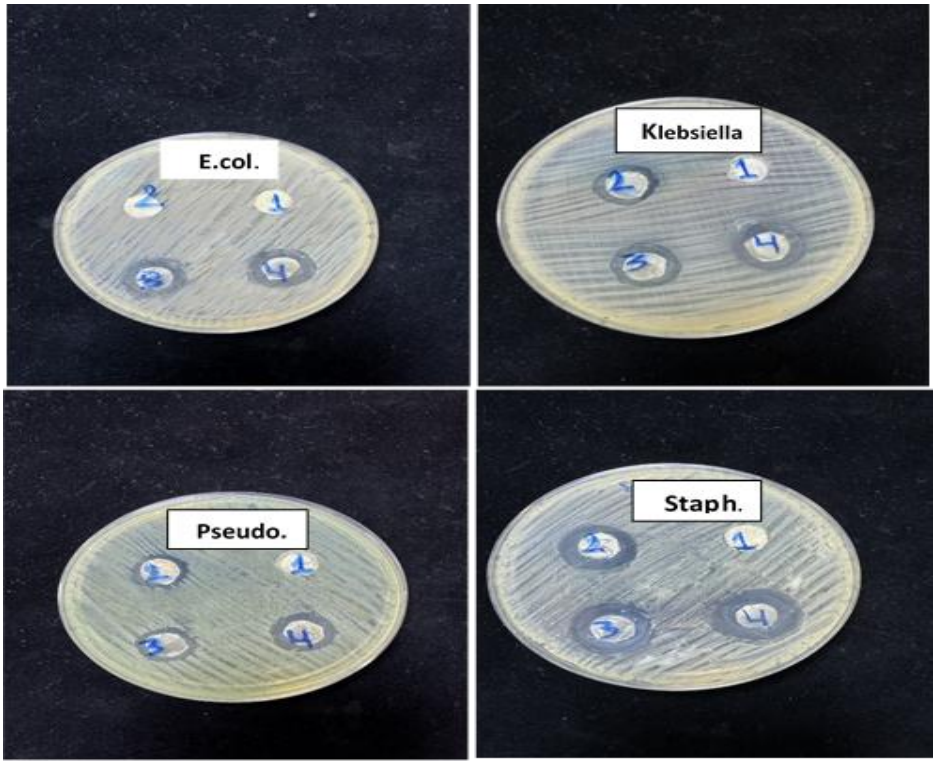

Figure 10 Antibacterial activity for PMMA and 3 different mixed (TiO_2-ZrC) NCs.

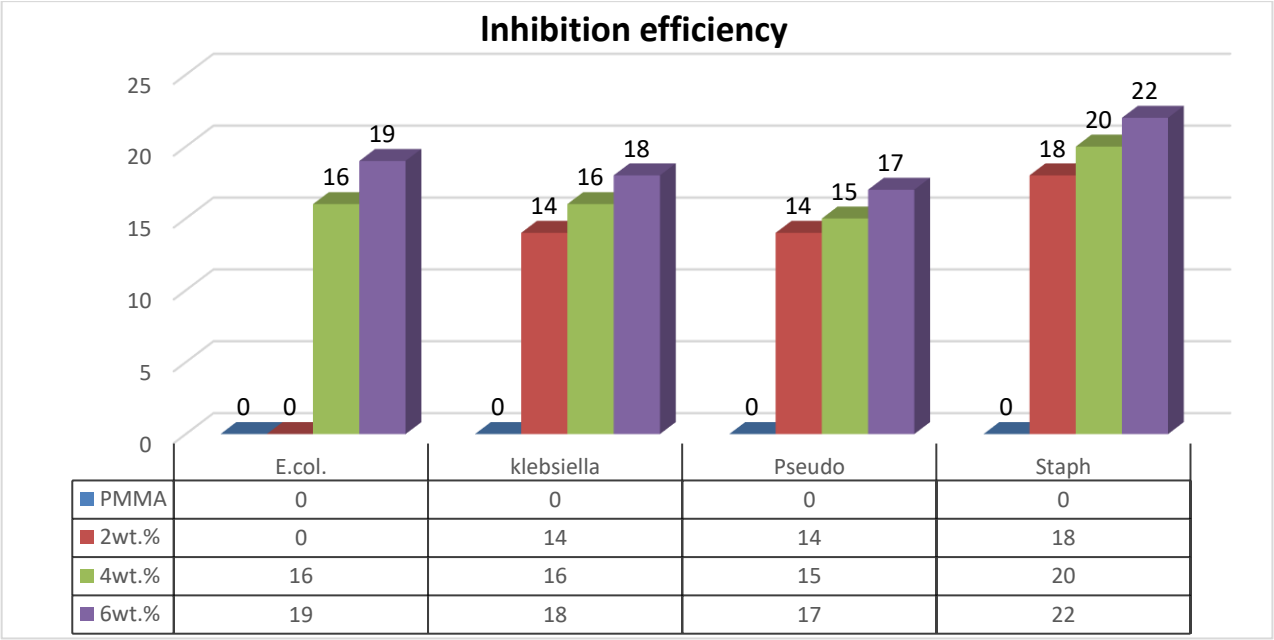

	E.col.	klebsiella	Pseudo	Staph
PMMA	0	0	0	0
2wt.%	0	14	14	18
4wt.%	16	16	15	20
6wt.%	19	18	17	22

Figure 11 The effect of contain (TiO_2-ZrC) NCs on inhibiting the growth of 4 bacterial strains.

Conclusions

A successful attempt was made to fabricate PMMA/(TiO_2-ZrC) nanofiber composites through electrospinning. The physical interaction between PMMA and (TiO_2-ZrC) was approved through FTIR analysis. FESEM images verified that the electrospun PMMA and its composite nanofibers measured between 82.37 and 139.59 nm. The reduction in light transmittance in the UV spectrum is a favorable indicator of the protective function in solar cells. The allowed and forbidden transitions decreased from 3.5 and 3.2 eV (pure polymer) to 2.8 and 2.18 eV at the

mixture of TiO_2 and ZrC nano additives reached a weight of 6 %, which makes an encouraging sign for use in many optoelectronic devices. A study of the broad optical spectra indicated that the E_d, n_s, ε_s, M_{-1}, and M_{-3} increased with increasing (TiO_2-ZrC) content. The greatest inhibition zone of gram-positive (Staphylococcus aureus) bacteria was about 22 mm at a weight of 6 %, making it usable as an alternative to conventional antibiotics.

Acknowledgements

Thanks to University of Babylon, Iraq for support.

References

[1] FS Hashim, MH Almaamori and FJ Hamood. Effect of silica on the mechanical properties of rubber reclaim composite. *International Journal of ChemTech Research* 2016; **9(4)**, 325-333.

[2] G Kim, GH Michler, F Ania and FJB Calleja. Temperature dependence of polymorphism in electrospun nanofibres of PA6 and PA6/clay nanocomposite. *Polymer* 2007; **48(16)**, 4814-4823.

[3] Y Ji, B Li, S Ge, JC Sokolov and MH Rafailovich. Structure and nanomechanical characterization of electrospun PS/Clay nanocomposite fibers. *Langmuir* 2006; **22(3)**, 1321-1328.

[4] Y Gao, J Zhang, J Liang, D Yuan and W Zhao. Research progress of poly(methyl methacrylate) microspheres: Preparation, functionalization and application. *European Polymer Journal* 2022; **175**, 111379.

[5] SUM Khan, M Al-Shahry and WB Ingler. Efficient photochemical water splitting by a chemically modified n-TiO 2. *Science* 2002; **297(5590)**, 2243-2245.

[6] I Chung, I Park, K Seung-Hyun, M Thiruvengadam and G Rajakumar. Plant-Mediated synthesis of silver nanoparticles: Their characteristic properties and therapeutic applications. *Nanoscale Research Letters* 2016; **11**, 40.

[7] AM Bannunah. Biomedical applications of zirconia-based nanomaterials: Challenges and future perspectives. *Molecules* 2023; **28(14)**, 5428.

[8] X Wei, C Back, O Izhvanov, OL Khasanov, CD Haines and EA Olevsky. Spark plasma sintering of commercial zirconium carbide powders: Densification behavior and mechanical properties. *Materials* 2015; **8(9)**, 6043-6061.

[9] Z Huang, Y Zhang, M Kotaki and S Ramakrishna. A review on polymer nanofibers by electrospinning and their applications in nanocomposites. *Composites Science and Technology* 2003; **63(15)**, 2223-2253.

[10] MM Abbas, A Abdulridha, AK Jassim and F Hashim. Physical properties of nanoparticles Nd added Bi1.7Pb0.3Sr2Ca2Cu3Oy superconductors. *AIP Conference Proceedings* 2018; **1968(1)**, 030009.

[11] Y Chen, Z Zhang, J Yu and Z Guo. Poly(methyl methacrylate)/silica nanocomposite fibers by electrospinning. *Journal of Polymer Science Part B: Polymer Physics* 2009; **47(12)**, 1211-1218.

[12] N Kanth, W Xu, U Prasad, D Ravichandran, AM Kannan and K Song. PMMA-TiO2 fibers for the photocatalytic degradation of water pollutants. *Nanomaterials* 2020; **10(7)**, 1279.

[13] N Salloomi, NH Ali, HS Rasheed and TJ Alwan. Nanofibers of PMMA/TiO2 produced by electrospinning. *Mustansiriyah Journal of Pure and Applied Sciences* 2025; **3(1)**, 117-122.

[14] FJ Tommasini, LAC Ferreira, LGP Tienne, VDO Aguiar, MHPD Silva, LFDM Rocha and MDFV Marques. Poly (methyl methacrylate)-SiC nanocomposites prepared through in situ polymerization. *Materials Research* 2018; **21(6)**, e20180086.

[15] L Torrisi, AM Roszkowska, L Silipigni, M Cutroneo and A Torrisi. Effects of 365 nm UV lamp irradiation of polymethylmethacrylate (PMMA). *Radiation Effects and Defects in Solids* 2024; **179(1-2)**, 264-274.

[16] U Ali, KJBA Karim and NA Buang. A Review of the properties and applications of poly (methyl methacrylate) (PMMA). *Polymer Reviews* 2015; **55(4)**, 678-705.

[17] CB Godiya, S Gabrielli, S Materazzi, MS Pianesi, N Stefanini and E Marcantoni. Depolymerization of waste poly(methyl methacrylate) scraps and purification of depolymerized products. *Journal of Environmental Management* 2019; **231**, 1012-1020.

[18] DCL Vasconcelos, VC Costa, EHM Nunes, ACS Sabioni, M Gasparon and WL Vasconcelos. Infrared spectroscopy of titania sol-gel coatings on 316L stainless steel. *Materials Sciences and Applications* 2011; **02(10)**, 1375-1382.

[19] M Iorio, J Teno, M Nicolas, R Garcia-Gonzalez, VH Pelaez, G Gonzalez-Gaitano and J Gonzalez-Benito. Conformational changes on PMMA induced by the presence of TiO2 nanoparticles and the processing by Solution Blow Spinning. *Colloid and Polymer Science* 2018; **296**, 461-469.

[20] C Liu, L Zhang, X Li, X Chang, Y Wu and X Wang. Synthesis, characterization, and ceramization of a carbon-rich SiCw-ZrC-ZrB2 preceramic polymer precursor. *Ceramics International* 2019; **45(13)**, 16097-16104.

[21] E Jamroz, P Kulawik and P Kopel. The effect of nanofillers on the functional properties of biopolymer-based films: A review. *Polymers* 2019; **11(4)**, 675.

[22] CM Mathew, K Kesavan and S Rajendran. Structural and electrochemical analysis of PMMA based gel electrolyte membranes. *International Journal of Electrochemistry* 2015; **2015(1)**, 494308.

[23] AI Abdelamir, E Al-Bermany and FS Hashim. Enhance the optical properties of the synthesis PEG/Graphene- based nanocomposite films using GO nanosheets. *Journal of Physics: Conference Series* 2019; **1294**, 022029.

[24] MR Khaleel, FS Hashim and AHO Alkhayatt. Impact of pH and ZnO NPs on the fabricated PVA-PVP/ZnO nanofibers: Morphology, absorption behavior, anticancer, and antibacterial activity. *Ceramics International* 2024; **50(20)**, 40161-40170.

[25] MY Abbas and FS Hashim. Electrospinning preparation of PVP/Ni2O3 nanofibers: Characterization and antibacterial studies. *AIP Conference Proceedings* 2024; **3229**, 110007.

[26] MR Khaleel, FS Hashim and AHO Alkhayatt. Preparation, characterization and the antibacterial activity of PVA-PVP/Co3O4 nanofiber films via indigenous electrospinning setup. *AIP Conference Proceedings* 2024; **3229**, 090002.

[27] J Tauc. Amorphous semiconductors. *Physics Today* 1976; **29(10)**, 23-31.

[28] MH Rasheed, FS Hashim and KH Abass. Impact of Ag nanoparticles on the spectral and optical properties of electrospun nanofibrous poly(vinyl alcohol)–Poly(acrylamide). *International Journal of Nanoscience* 2023; **22(3)**, 2350025.

[29] FS Hashim, SA Jabbar, E Al-Bermany and K Abdali. Effect of inclusion ZnO-Co3O4 nanoparticles on the microstructural and optical properties of PVA-CMC polymeric blend for biomedical, uv shielding, and nuclear radiation shielding applications. *Plasmonics* 2024; **20**, 1629-1641.

[30] RA Ghazi, KH Al-Mayalee, E Al-Bermany, FS Hashim and AKJ Albermany. Impact of polymer molecular weights and graphene nanosheets on fabricated PVA-PEG/GO nanocomposites: Morphology, sorption behavior and shielding application. *AIMS Materials Science* 2022; **9(4)**, 584-603.

[31] MM Abutalib and A Rajeh. Boosting optical and electrical characteristics of polyvinyl alcohol/carboxymethyl cellulose nanocomposites by GNPs/MWCNTs fillers as an application in energy storage devices. *International Journal of Energy Research* 2022; **46(5)**, 6216-6224.

[32] P Priyadarshini, D Alagarasan, R Ganesan, S Varadharajaperumal and R Naik. Influence of proton ion irradiation on the linear–nonlinear optoelectronic properties of Sb 40 Se 20 S 40 thin films at different fluences for photonic devices. *ACS Applied Optical Materials* 2023; **1(1)**, 55-68.

[33] S Das, S Senapati, D Alagarasan, S Varadhrajaperumal, R Ganesan and R Naik. Thermal annealing-induced transformation of structural, morphological, linear, and nonlinear optical parameters of quaternary As 20 Ag 10 Te 10 Se 60 thin films for optical applications. *ACS Applied Optical Materials* 2023; **1(1)**, 17-31.

[34] F Yakuphanoglu, A Cukurovali and I Yilmaz. Determination and analysis of the dispersive optical constants of some organic thin films. *Physica B: Condensed Matter* 2004; **351(1-2)**, 53-58.

[35] N Idil, S Aslıyuce, I Percin and B Mattiasson. Recent advances in optical sensing for the detection of microbial contaminants. *Micromachines* 2023; **14(9)**, 1668.

[36] HH Jassim and FS Hashim. Synthesis of (PVA/PEG: ZnO and Co3O4) nanocomposites: Characterization and antibacterial studies. *AIP Conference Proceedings* 2022; **2398**, 020033.

[37] AC Alavarse, FWDO Silva, JT Colque, VMD Silva, T Prieto, EC Venancio and J Bonvent. Tetracycline hydrochloride-loaded electrospun nanofibers mats based on PVA and chitosan for wound dressing. *Materials Science and Engineering: C* 2017; **77**, 271-281.

[38] FS Hashim, SH Idres, AN Tuama and K Abdali. Microstructure, optical, and antibacterial features of PVP/Cu2O electrospun nanofibers for optoelectronics and biological purposes. *Journal of Inorganic and Organometallic Polymers and Materials* 2024; **34**, 5342-5350.

[39] DA Sabur, A Hashim and MA Habeeb. Fabrication and exploration the structural and optical properties of Sb2O3-GO nanostructures doped PMMA-PC for photodegradation of pollutants dyes. *Optical and Quantum Electronics* 2023; **55**, 457.